ON THE LARGE-EDDY SIMULATION OF A FULLY DEVELOPED WIND-TURBINE ARRAY BOUNDARY LAYER

***D.Folch*[1], *F.X.Trias*[1], *and A.Oliva*[1]**

[1] ***Heat and Mass Transfer Technological Center, Technical University of Catalonia***
C/Colom 11, 08222 Terrassa (Barcelona)
david.folch@upc.edu

Abstract

Direct numerical simulations of the incompressible Navier-Stokes equations at high Reynolds numbers are not yet feasible, so dynamically less complex mathematical formulations such as Large Eddy Simulation (LES) have been developed. For the well-known eddy-viscosity models for LES, the computational method is based on the combination of invariants of a symmetric tensor that depends on the gradient of the resolved velocity field, $\mathsf{G} = \nabla\overline{\boldsymbol{u}}$. Several models (namely S3PQR) have been developed using the first three principal invariants of the symmetric tensor $\mathsf{G}\mathsf{G}^T$ with excellent results. Therefore, in this work, we will focus on the application of the S3PQR and other LES models on the free boundary layer case. Then, we will test their performances over a fully developed boundary layer wind farm, using a simplified wind turbine model.

1 Introduction

Large Eddy Simulation (LES) equations result from applying a spatial filter to the incompressible Navier-Stokes equations, yielding:

$$\begin{aligned} \partial_t\overline{\boldsymbol{u}} + C(\overline{\boldsymbol{u}},\overline{\boldsymbol{u}}) &= D(\overline{\boldsymbol{u}}) - \nabla p - \nabla\cdot\tau(\overline{\boldsymbol{u}}); \quad (1)\\ \nabla\cdot\overline{\boldsymbol{u}} &= 0 \end{aligned}$$

where $\overline{\boldsymbol{u}}$ is the filtered velocity and $\tau(\overline{\boldsymbol{u}})$ is the subgrid stress (SGS) tensor that approximates the effect of the under-resolved scales.

This equation needs a closure model to be numerically solved. The LES closure is of the type $\tau(\overline{\boldsymbol{u}}) \approx -2\nu_e S(\overline{\boldsymbol{u}})$ where $S(\overline{\boldsymbol{u}}) = 1/2(\nabla\overline{\boldsymbol{u}} + \nabla\overline{\boldsymbol{u}}^T)$ is the rate-of-strain tensor. We must define an eddy viscosity: $\nu_e = (C_m\Delta)^2 D_m(\overline{\boldsymbol{u}})$ where C_m is the model constant, Δ is the subgrid characteristic length, and $D_m(\overline{\boldsymbol{u}})$ is the differential operator with units of frequency associated with the model (Nicoud, Toda, et al. (2011)).

Most of the models of the LES algorithms are based on combinations of invariants of some tensor depending on the gradient of the velocity. The Smagorinsky (1963) model, Vreman (2004), WALE (Nicoud and Ducros (1999)), or the S3PQR models (Trias, Folch, A. Gorobets, et al. (2015)) are examples thereof. From the several mathematical invariants that can be calculated from the gradient tensor $\mathsf{G} = \nabla\overline{\boldsymbol{u}}$, besides $P_\mathsf{G} = tr(\mathsf{G})$ we will restrict ourselves on

$$\{Q_\mathsf{G}, R_\mathsf{G}, Q_\mathsf{S}, R_\mathsf{S}, V_\mathsf{G}^2\}$$

where, given this second-order tensor G, one can define

$$\begin{aligned} Q_\mathsf{G} &= (1/2)(tr^2(\mathsf{G}) - tr(\mathsf{G}^2)) \quad (2)\\ R_\mathsf{G} &= det(\mathsf{G})\\ Q_\mathsf{S} &= (1/2)(tr^2(\mathsf{S}) - tr(\mathsf{S}^2))\\ R_\mathsf{S} &= det(\mathsf{S})\\ V_\mathsf{G}^2 &= 4(tr(S^2\Omega^2) - 2Q_S Q_\Omega) \end{aligned}$$

with $\mathsf{S} = 1/2(\mathsf{G} + \mathsf{G}^T)$ and $\Omega = 1/2(\mathsf{G} - \mathsf{G}^T)$ as the symmetric and the skew-symmetric parts of the gradient tensor, respectively. For every incompressible flux, any invariant can be written as a function of the five so defined.

Then, the LES models can be written as:

- Smagorinsky model $\nu_e^{Smag} = f(Q_\mathsf{S})$
- Verstappen (2011) model $\nu_e^{Ve} = f(R_\mathsf{S}, Q_\mathsf{S})$
- WALE model $\nu_e^{W} = f(Q_\mathsf{G}, V, Q_\mathsf{S})$
- Vreman's model $\nu_e^{Vr} = f(V, Q_\mathsf{G}, Q_\Omega, Q_\mathsf{S})$
- σ-model $\nu_e^{\sigma} = f(\lambda_1, \lambda_2, \lambda_3)$ where $\lambda_1, \lambda_2, \lambda_3$ are the $\mathsf{G}\mathsf{G}^T$ tensor eigenvalues; Nicoud, Toda, et al. (2011)

One can construct new models that involve three types of invariants of the symmetric tensor $\mathsf{G}\mathsf{G}^T$, formally based on the lowest-order approximation of the subgrid stress tensor (Clark, Ferziger, and Reynolds (1979)).

$$\tau(\overline{\boldsymbol{u}}) = \frac{\Delta^2}{12}\mathsf{G}\mathsf{G}^T + \mathcal{O}(\Delta^4) \quad (3)$$

These invariants are directly related to the previous ones:

$$\begin{aligned} P_{\mathsf{G}\mathsf{G}^T} &= tr(\mathsf{G}\mathsf{G}^T) = 2(Q_\Omega - Q_\mathsf{S}) \quad (4)\\ Q_{\mathsf{G}\mathsf{G}^T} &= 2(Q_\Omega - Q_\mathsf{S})^2 - Q_\mathsf{G}^2 + 4tr(\mathsf{S}^2\Omega^2)\\ R_{\mathsf{G}\mathsf{G}^T} &= det(\mathsf{G}\mathsf{G}^T) = det(\mathsf{G})det(\mathsf{G}^T) = R_\mathsf{G}^2 \end{aligned}$$

The general form can be written as:

$$\nu_e = (C_{s3pqr}\Delta)^2 P_{\mathsf{G}\mathsf{G}^T}^p Q_{\mathsf{G}\mathsf{G}^T}^q R_{\mathsf{G}\mathsf{G}^T}^r \quad (5)$$

The different types of S3PQR models were obtained by restricting them to solutions with only two of those invariants:

$$\nu_e^{S3PQ} = (C_{s3pq}\Delta)^2 P_{\mathsf{GG}^T}^{-5/2} Q_{\mathsf{GG}^T}^{3/2} \quad (6)$$

$$\nu_e^{S3PR} = (C_{s3pr}\Delta)^2 P_{\mathsf{GG}^T}^{-1} R_{\mathsf{GG}^T}^{1/2} \quad (7)$$

$$\nu_e^{S3QR} = (C_{s3qr}\Delta)^2 Q_{\mathsf{GG}^T}^{-1} R_{\mathsf{GG}^T}^{5/6} \quad (8)$$

or for simplicity, PQ, PR, QR.

There are two ways to determine the remaining model constant:

1. Imposing numerical stability and less or equal dissipation than Vreman's model. Then,

$C_{s3pq} = C_{s3pr} = C_{s3qr} = \sqrt{3}C_{Vr} \approx 0.458$

2. Granting that the averaged dissipation of the models is equal to that of the Smagorinsky model. Then,

$C_{s3pq} = 0.572$, $C_{s3pr} = 0.709$, $C_{s3qr} = 0.762$

Therefore, and finally, there are six possible combinations to test (3 model types x 2 constants) that we will call PQ1, PQ2, and so on, in this article.

Depending on the constant chosen, there have been found differences in the numerical results. For example, simulations of decaying isotropic turbulence have shown that only the type 2 constant values provide the right SGS dissipation (Trias, Folch, A. Gorobets, et al. (2015)).

Another important property of each of the S3PQR models is its 2D behavior: only R_{GG^T}-dependent models switch off for 2D flows, so we may expect that S3PR and S3QR models would adjust better in our current cases.

Further key characteristics are positiveness, locality, Galilean invariance, and proper near-wall $\mathcal{O}(y^3)$ dependence on normal direction (Chapman and Kuhn (1986)).

To assure the validity of the models, and to discriminate between them, they have been already tested on benchmark cases like the channel flow (Trias, A. Gorobets, and Oliva (2013)), and also compared with the DNS of Moser, Kim, and Mansour (1999)); and the homogeneous isotropic turbulence (Trias, Folch, A. Gorobets, et al. (2015), both in the decaying and forced simulations, compared with classical Comte-Bellot and Corrsin (1971) experiment, giving excellent results.

Note that there also could be technical specifications of the algorithm that could yield different performances of the model. That is, for example, the time-stepping procedure, the characteristic of the domain, or the mathematical approximations.

2 Model Layout and Results

For all the current computations of this work, the grid size of the domain is $Nx = 32$, $Ny = 64$, and $Nz = 32$ points, where x, y, and z, are the streamwise, wall-normal, and spanwise directions. The Reynolds number is fixed along the simulation to $Re_{\delta^*} = 1000$, where δ^* is the displacement thickness.

Pseudo-spectral methods provide high resolution when working with derivatives and have been seen as a very good tool for cases where periodic conditions could be applied. Indeed, pseudo-spectral algorithms, by construction, demand strict periodic conditions (Boyd (2001)). But one of the main features of the boundary layer case is that it continually develops over the streamwise direction. To solve this issue, the general algorithm for our boundary layer is based on the method proposed by Spalart and Leonard (1987), which includes normal coordinate similarity transformations, growing terms $GT(\overline{\boldsymbol{u}}, \overline{U})$ and scaling factors.

There are some differences with our (pseudo-spectral) implementation, though. First, our algorithm is based on the strong formulation of the Navier-Stokes equations with a Poisson - pressure correction term. Second, we use the standard algebraic scaling (Boyd (2001)), $y_\infty = L\frac{1+y}{1-y}$, for the the semi-infinite domain over the normal direction. Finally, the computation relies on a fully explicit second-order time-integration method (Trias, Folch, A. Gorobets, et al. (2019)). We will test the zero mean pressure gradient case.

Boundary layer

First, we deal with the free boundary layer cases without the turbine model. To compare the LES models and Spalart and Leonard (1987) results, we can list three main parameters: u_τ as the friction velocity, H as the ratio of the displacement thickness to the momentum thickness, and κ as the Von Kármán constant (see Table 1, where Sp-Le stands for the reference values).

Case:	u_τ	H	κ
Sp-Le DNS	**0.049**	**1.52**	**0.39**
No model	0.049	1.61	0.35
Vreman	0.050	1.51	0.47
WALE	0.046	1.54	0.47
PQ1	0.048	1.58	0.35
PR1	0.050	1.54	0.44
QR1	0.049	1.57	0.35
PQ2	0.046	1.57	0.42
PR2	0.049	1.53	0.39
QR2	0.048	1.57	0.32

Table 1: boundary layer characteristic parameters calculated for each model. First line results from reference. Grid size for all the other cases: 32x64x32

The Smagorinsky method did not yield meaningful results with the current algorithm (incorrect near-wall behavior). The rest of the LES models give reasonable results. All of the S3PQR cases present comparable values, with PR2 standing as nearly the best in the global analysis. As an example of the performance of this model, we plot the velocity profile and the root mean square of the velocities (Figure 1). The main differences between the models can be seen in plot-

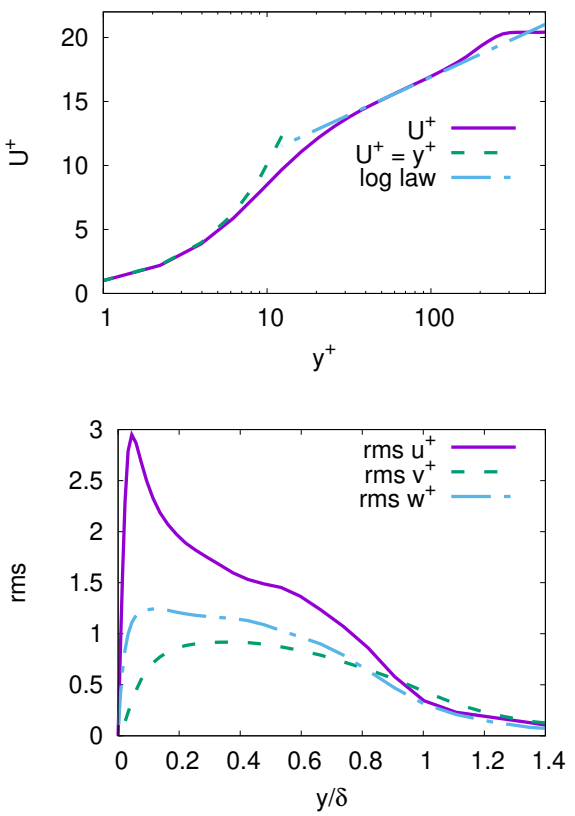

Figure 1: Case PR2, present results. Top: normalized average streamwise velocity profile, U^+; law of the wall, $U^+ = y^+$; log law. Bottom: rms u^+; rms v^+; rms w^+; δ is the boundary layer thickness

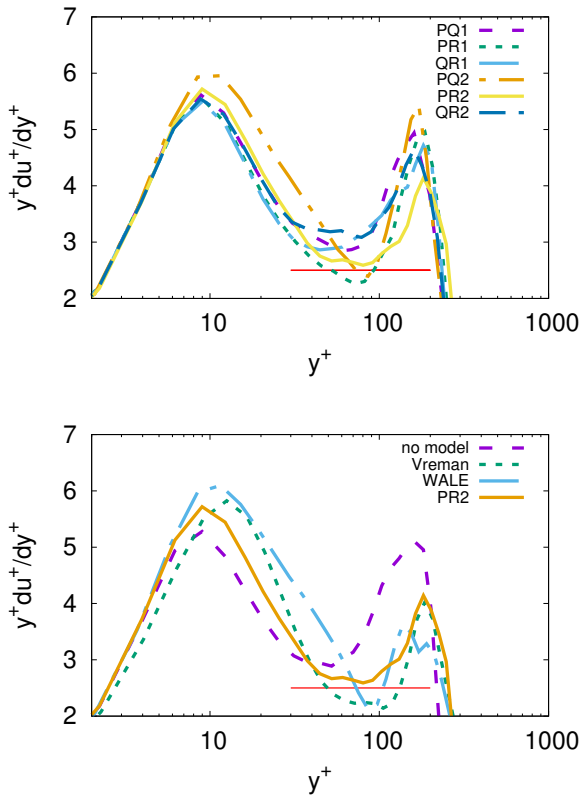

Figure 2: y^+du^+/dy^+ vs y^+. Top: S3PQR models. Bottom: comparison with other LES models. The horizontal line marks the point(s) where the log law would be with $\kappa = 0.4$

ting the derivative of the velocity profile y^+du^+/dy^+ (see Figure 2). As Spalart (1988) recalls in his work, the logarithmic layer corresponds to the minimum, and the value of κ is thus determined, despite the noise due to the lack of resolution. Moreover, the values of the maxima can be directly compared with that of Spalart. Then we can confidently say that S3PQR models capture the general trend. Besides, the PR2 model values are within the range of the expected ones. Moreover, PR2 also performs better than Vreman, WALE, or no-model algorithms.

We can also plot the rms u^+ values for all of them (Figure 3) yielding apparently no further discrimination between the models, but as a demonstration of their similar performance.

Thus so far, for the S3PQR models, we have obtained reliable results with low computational effort for the free boundary layer.

Wind farm

We will follow the model used by Calaf, Meneveau, and Meyers (2010) which is based on the concept of a disk actuator for every wind turbine. The force of the turbine (per unit mass), in the streamwise direction, at a given grid point i, j, k, is given by

$$F(i,j,k) = -\frac{1}{2} C'_T \langle \overline{\boldsymbol{u}}^T \rangle_d^2 \frac{\gamma_{j,k}}{\Delta x}$$

where C'_T is a thrust coefficient, $\langle \overline{\boldsymbol{u}}^T \rangle_d^2$ is the disk local averaged velocity, $\gamma_{j,k}$ is the fraction area overlap of the disk and Δx is the distance between turbines. This disk actuator model can be straightforwardly applied to our algorithm. We will compute our wind farm with the same number and array geometry of the turbines that a specific case of the reference: 24 disk actuators evenly distributed in four rows and six columns.

However, all the other configuration parameters, like the Reynolds number, energy supply, and wall boundary conditions, are different. So, at this moment the comparison can only rely on the general behavior of the vertical profiles and the magnitude orders of the values.

The adaptation of Spalart's boundary layer method to that of the wind farm poses some challenges. The growing terms of Spalart that supply energy to the system rely on the existence of one single log law and its transition to a velocity defect law. The main parameter is friction velocity. In the case of the wind farm, we expect two log laws (Calaf, Meneveau, and Meyers (2010)) with two defined friction velocities. The solution adopted in this case is simply an average between the two friction velocities, so the error for the growing terms is, at least, reasonably bounded. In Figure 4, on top, we show the results for the velocity profile with

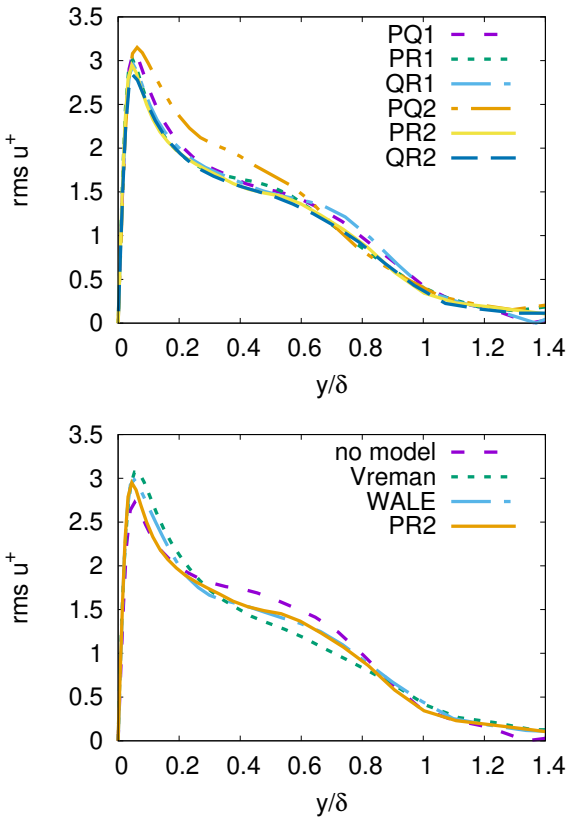

Figure 3: rms u^+. Top: S3PQR models. Bottom: comparison with other LES models

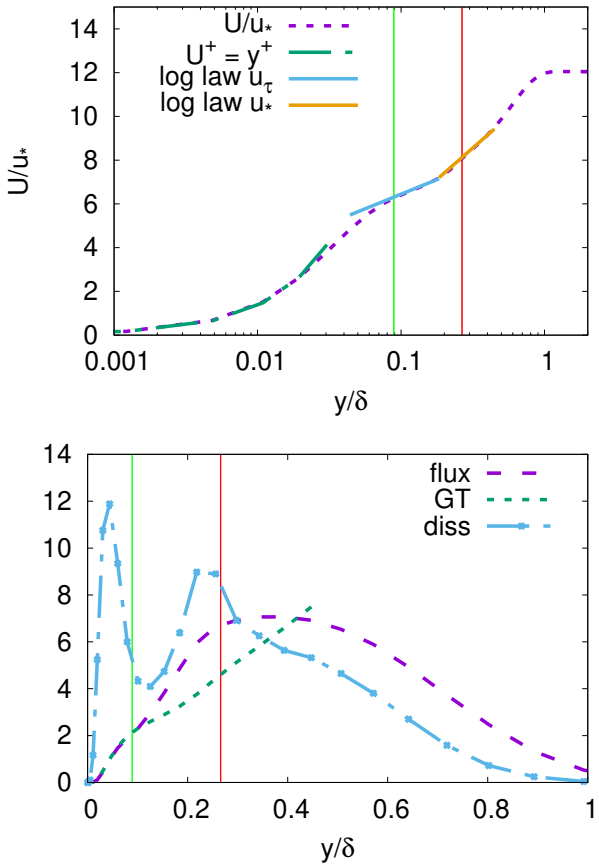

Figure 4: Model PR2 as an example. Top: average streamwise velocity. The green vertical line is the position of the bottom of the turbine hub. The red line is the top. Note the law of the wall and the two log laws. Bottom: Normalized mean kinetic energy contributions: **flux**, $\delta\Phi = - < uv > U/u_*^3$; **GT**, normalized growing terms; **diss**, $- < uv > \partial_y U/(u_*^3/\delta)$

PR2. On the bottom, some energy terms values.

Some of the several quantities that may be of interest are listed in Table 2 and Table 3. All of them are also computed in Calaf, Meneveau, and Meyers (2010). The meaning of the terms is as follows:

i) Table 2, quantities related to velocity profiles: $z0_{Hi}/zH$, as the ratio of the effective roughness above the turbine hub and the height of the turbines' center (it should be written $y0_{Hi}/yH$ but we used the reference nomenclature); u_τ, the usual friction velocity at the wall; u_*, the computed friction velocity above the hub;

ii) Table 3, quantities related to energy: P, the time and horizontally averaged power extracted for every turbine; W_t, the time, horizontally, and vertically (along the hub) averaged power; $\delta\Phi$, the vertical flux of kinetic energy. Finally, the term EB (for energy budget) is the balance between all the energy contribution terms. For a perfect match, it should be 100% (the reference achieves 98%). As it can be seen, all the magnitudes are of the same order as reference. From the column of $P/\delta\Phi$, it seems that it also reproduces the observed behavior that the wind turbines, in a fully developed boundary layer regime, extract kinetic energy through vertical fluxes.

As said before, we can expect two well-defined log laws along the vertical velocity profile, represented as two minima in the y^+du^+/dy^+ vs y^+ plot. In the present algorithm and configuration, QR1 and no-

MODEL	$z0_{Hi}/zH$	u_τ	u_*	u_τ/u_*
no model	0.160	0.051	0.109	0.47
Vreman	0.072	0.056	0.085	0.66
WALE	0.082	0.050	0.089	0.56
PQ1	0.096	0.052	0.092	0.57
PR1	0.105	0.052	0.094	0.55
QR1	0.123	0.052	0.100	0.52
PQ2	0.074	0.052	0.085	0.61
PR2	0.065	0.052	0.083	0.63
QR2	0.098	0.052	0.093	0.56

Table 2: some velocity profile related quantities of a wind farm simulation. Grid size:32x64x32

model fail to yield these two log laws, while PQ1 and PR1, barely do. Despite this, for them, we have calculated the values as if there were a log law in the same approximate position as it appears in the other models (see Figure 5). The remaining ones fulfill this condition, as can be seen in the same figure. The lack of this

MODEL	$P/\delta\Phi$	$W_t/\delta\Phi$	EB
no model	0.68	0.81	94%
Vreman	0.67	0.78	94%
WALE	0.79	0.90	94%
PQ1	0.75	0.86	96%
PR1	0.74	0.85	95%
QR1	0.73	0.84	95%
PQ2	0.75	0.86	95%
PR2	0.77	0.88	97%
QR2	0.74	0.86	95%

Table 3: energy-related quantities of a wind farm simulation

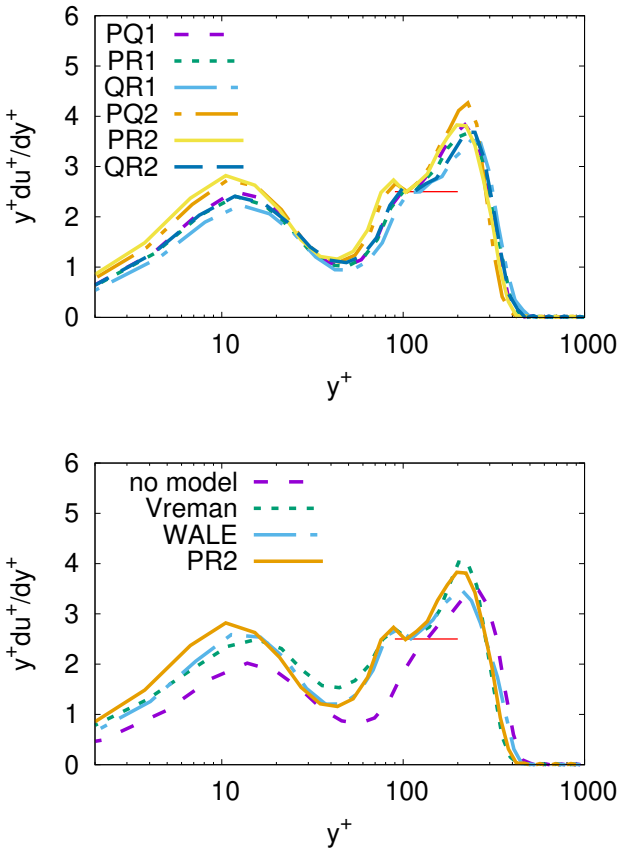

Figure 5: y^+du^+/dy^+. All the values normalized by u_*; Top: S3PQR models. Bottom: other LES models. Note the presence of one or two minima corresponding to the log laws. The horizontal line shows the expected second log law with, by definition, $\kappa = 0.4$ Note too, that in cases where it is present, it appears approximately in the same position

second log law could be due again to noise (the derivative is more sensitive to it), low resolution, or intrinsic behavior of the models. The question remains open to future work.

3 Conclusions

Without benchmark values for this wind farm particular case, it is not possible to assess confidently which model gives better results or whether S3PQR algorithms are better than other LES models because all of them (except maybe the no-model) are in the same range of values. See as an example Figure 6. Despite this, for most of them, we have seen that the general behavior matches reasonably that of reference. Therefore, we can say at this moment that at least the S3PQR type 2 algorithms are well-suited for both free boundary layer and wind farm simulations.

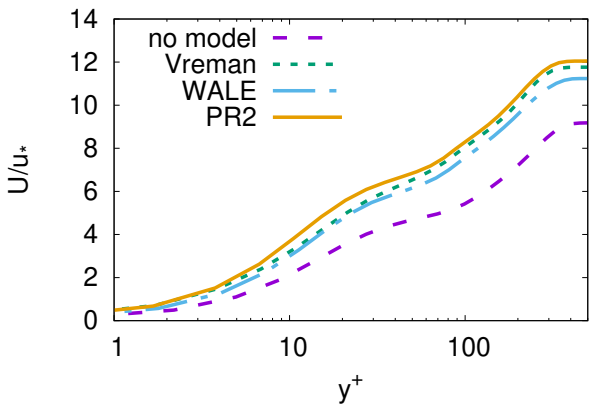

Figure 6: Velocity profiles. Some LES models. The other S3PQR models follow nearly the same pattern as PR2.

Acknowledgments

This project is supported by the *Ministerio de Economía y Competitividad*, Spain, RETOtwin project (PDC2021-120970-I00).

References

Boyd, John P. (2001). *Chebyshev and Fourier Spectral Methods*. Dover Publications, Inc.

Calaf, M., C. Meneveau, and J. Meyers (2010). "Large eddy simulation study of fully developed wind-turbine array boundary layers". In: *Physics of Fluids* 22, p. 015110.

Chapman, D. R. and G. D. Kuhn (1986). "The limiting behaviour of turbulence near a wall". In: *Journal of Fluid Mechanics* 170, pp. 265–292.

Clark, R. A., J. H. Ferziger, and W. C. Reynolds (1979). "Evaluation of subgrid-scale models using an accurately simulated turbulent flow". In: *Journal Fluid Mechanics* 91, pp. 1–16.

Comte-Bellot, G. and S. Corrsin (1971). "Simple Eulerian time correlation of full- and narrow-band velocity signals in grid-generated, isotropic turbulence". In: *Journal of Fluid Mechanics* 48, pp. 273–337.

Moser, R. D., J. Kim, and N. N. Mansour (1999). "Direct numerical simulation of turbulent channel flow up to $Re_\tau = 590$". In: *Physics of Fluids* 11 (4), pp. 943–945.

Nicoud, F. and F. Ducros (1999). “Subgrid-scale stress modelling based on the square of the velocity gradient tensor”. In: *Flow, Turbulence and Combustion* 62.3, pp. 183–200.

Nicoud, F., H. B. Toda, et al. (2011). “Using singular values to build a subgrid-scale model for large eddy simulations”. In: *Physics of Fluids* 23.8, p. 085106.

Smagorinsky, J. (1963). “General Circulation Experiments with the Primitive Equations”. In: *Monthly Weather Review* 91, pp. 99–164.

Spalart, P.R. (1988). “Direct simulation of a turbulent boundary layer up to $R_\theta = 1410$”. In: *Journal of Fluid Mechanics* 187, pp. 61–98.

Spalart, P.R. and A. Leonard (1987). *Direct Numerical Simulation of Equilibrium Turbulent Boundary Layers*. Berlin: Springer-Verlag, pp. 234–252.

Trias, F. X., D. Folch, A. Gorobets, et al. (2019). “Spectrally-consistent regularization of Navier-Stokes equations”. In: *Journal of Scientific Computing* 79, pp. 992–1014.

Trias, F. X., D. Folch, A. Gorobets, et al. (2015). “Building proper invariants for eddy-viscosity subgrid-scale models”. In: *Physics of Fluids* 27.6, p. 065103.

Trias, F. X., A. Gorobets, and A. Oliva (2013). “A simple approach to discretize the viscous term with spatially varying (eddy-)viscosity”. In: *Journal of Computational Physics* 253, pp. 405–417.

Verstappen, R. (2011). “When does eddy viscosity damp subfilter scales sufficiently?” In: *Journal of Scientific Computing* 49.1, pp. 94–110.

Vreman, A. W. (2004). “An eddy-viscosity subgrid-scale model for turbulent shear flow: Algebraic theory and applications”. In: *Physics of Fluids* 16.10, pp. 3670–3681.